Magnonic Aharonov-Casher effect and electric field control of chirality-dependent spin-wave dynamics in antiferromagnets

O. O. Boliasova [1,2] and V. N. Krivoruchko [3]

[1] *State Research Institution, Kyiv Academic University, 36 Academician Vernadsky Boulevard, 03142 Kyiv, Ukraine*

[2] *G. V. Kurdyumov Institute for Metal Physics of the NAS of Ukraine, 36 Academician Vernadsky Boulevard, 03142 Kyiv, Ukraine*

[3] *Donetsk Institute for Physics and Engineering named after O. O. Galkin of the NAS of Ukraine, 46 Nauki Avenue, 03028 Kyiv, Ukraine*

(Received 28 July 2024; revised 24 March 2025; accepted 13 May 2025; published 23 May 2025)

Effective control of spin-wave (SW) dynamics is among the current topical goals of research in magnonics. Electric field control of SW dynamics in insulating magnetic materials by creating the Aharonov-Casher (AC) topological phase without energy dissipation due to joule heating is a highly preferred way. The AC phase is purely a quantum phenomenon and has no classical interpretation. It manifests as the electric-field-induced shift in the SW's phase, group velocity direction, and SW's attenuation. Within a linear approximation, the magnonic AC effect can be considered by adding a Dzyaloshinskii-Moriya-like interaction between neighboring spins, which is proportional to the magnitude and sign of the applied electric field. We study the topological AC effect on magnetization dynamics in two-sublattice easy-axis insulating antiferromagnets. The analytical calculation indicates that a static electric field is an effective tool for selectively and successfully manipulating right-handed and left-handed polarized SWs, their amplitude, and propagation length. Our theory also reveals the electric field effect on anomalous magnon dispersion characteristics—a superluminal-like propagation of magnons at nanoscale distances. We also make numerical evaluations for antiferromagnetic dielectric to illustrate the theoretical predictions. The AC topological effect gives an effective method for the chirality-selective manipulation of magnon dynamics and opens promising research directions and practical applications of antiferromagnets in magnonics.

DOI: 10.1103/PhysRevB.111.174440

I. INTRODUCTION

In recent years, spin-waves (SWs, magnons) have become promising candidates for carrying information in computing devices with ultralow power consumption, forming a separate physics field—magnonics [1,2]. Apart from the absence of joule heating during the propagation, another important feature of SWs is their applicability in a wide frequency range. For practical applications, frequency is an important parameter because it affects the speed of calculations. Among the key dynamic characteristics of SWs are the phase, amplitude, and propagation length. In this regard, one of the main goals in magnonics is to increase the efficiency of magnonic device operation by choosing materials and methods for controlling their functional characteristics. Compared to ferromagnets, antiferromagnets (AFMs) have the advantages of minimized stray fields and fast magnetization dynamics up to the terahertz range. Moreover, AFMs with collinear antiparallel-coupled magnetic moments in equilibrium (Néel order) are resistant to moderate magnetic fields, so the information in AFM memory devices is protected from damage by an external magnetic field. In addition, there are a lot of dielectrics, metallic, and semiconducting materials with antiferromagnetic order.

Compared to ferromagnets with only right-handed SWs, magnons in AFMs possess both right-handed (RH, counterclockwise) and left-handed (LH, clockwise) chirality, due to the antiparallel magnetic sublattices state [3,4]. The right- and left-hand polarized SWs could be used as the basic elements for encoding information, such as the spin-up and spin-down electrons in modern computers. Possessing these unique features, AFMs have a great perspective for applications in information technology (see recent reviews [5–10]). The main challenges for implementing AFMs in magnonic devices are uncovering the mechanisms of proper propagation, separate manipulation of the RH and LH SWs, and their detection. The ways to manipulate magnetic dynamics are actively discussed [11–15]. The energy of the RH and LH magnons is degenerate without any external fields. The mechanisms of the SWs splitting and manipulation of their dispersion and attenuation in AFMs by various methods are among the topics in connection to digital data processing realization utilizing AFMs. The most direct way is to apply an external magnetic field. However, a large field is usually required to obtain a moderate SWs' energy splitting.

Lee *et al.* [13] theoretically and numerically grounded that the RH and the LH SWs dispersion relations in an AFM will split into separate bands with specific polarities when crossing the wall of interfacial inhomogeneous Dzyaloshinskii-Moriya (DM) interaction. It has also been demonstrated that the

magnon spectrum can be split by combining the strain or the DM interaction with adiabatic spin-transfer torque effects. Kim *et al.* [14] have shown that circularly polarized magnon spectrum splitting occurs when magnons pass through a rotating domain wall. Recent studies of an electric current's spin-transfer torque effects (Slonczewski-type and Zhang-Li type) reveal a rather complex behavior concerning the relationship between the damping of the LH and the RH SWs and a way to control their polarization separately in AFM [15].

Electric current control of SW dynamics in conducting magnetics is among the topical goals of research in magnonics. When a spin-polarized current $\mathbf{j}$ is injected into a magnetic material, it exerts a torque on the local magnetic moment by transferring spin angular momentum and causing the current-induced SW Doppler shift. Vlaminck and Bailleul [16] experimentally detected in the metallic AFM $Ni_{80}Fe_{20}$ stripe the current-induced frequency shift $\Delta\omega \sim P\mathbf{jk} \sim P\mathbf{Ek}$ of SWs with a wave vector $\mathbf{k}$, where $\mathbf{E}$ is an external electric field and P is the degree of spin polarization of the electrical current. This current-induced frequency shift can be identified as the Doppler shift as an electron system drifts concerning the laboratory frame. The modification of SW dynamics in metallic AFM and in compensated ferrimagnetic by an electrical current that generates spin-transfer torques is theoretically predicted in Refs. [17] and [18], respectively.

Authors [19,20] proposed another possibility to control SW dynamics in collinear dielectric AFM. In insulating AFM magnons cannot be driven by an electric current. But, in collinear AFM the DM interaction breaks the left-handed and right-handed SWs' energy degeneracy causing a population imbalance between the number of magnons in spin-up and spin-down states and a population imbalance between the $\mathbf{k}$ and $-\mathbf{k}$ states. A temperature gradient ∇T courses a longitudinal magnon current and spin Nernst effect.

In Ref. [21], topological $\mathbf{E}$-field effects induced by a high-frequency laser on nonequilibrium magnon dynamics in the insulating AFM have been studied. The authors show that a linearly polarized laser can generate helical edge magnon states and induce the magnonic spin Nernst effect. In contrast, a circularly polarized laser can generate chiral edge magnon states and induce the magnonic thermal Hall effect. In work [22], the magnon spin photogalvanic effect caused by the Aharonov-Casher (AC) phase has been proposed as a mechanism in which magnons can be excited and directly controlled by an electric field of light. Spin current generation by applying a time-dependent $\mathbf{E}$ field due to the coupling between magnons and the electric field through the AC effect has also been discussed in a recent paper [23]. The authors demonstrate that a time-varying electric field can act as an efficient spin current generator and offer a promising platform for investigating magnonic topological effects.

The effects of the static electric field on magnetization dynamics in magnetic insulators has been proposed and actively discussed [24–26]. The effect of the external electric field on SW dynamics manifested in the form of an additional phase called the Aharonov-Casher phase [27], that is a special case of the Berry phase [28], is an example of the quantum topological of $\mathbf{E}$-field effects on the dynamic of neutral particles. It is manifested as a shift in dispersion and group velocity direction of SW's by an external electric field. In a linear approximation, the AC effect can be accounted for by adding a DM-like interaction between neighboring spins, the magnitude of which is proportional to the applied $\mathbf{E}$ field, the exchange coupling, and the spin-orbit coupling [25,26]. This is an example of a topological effect in quantum physics. According to the paradigm of quantum physics, the voltage control of static magnetic parameters (e.g., an anisotropy through strain-mediated magnetoelectric coupling) implies a modification of the local (Landau) system parameters. An example of a local-topological effect on magnetization dynamics is the behavior of magnons in magnets with artificial local magnetic structures, such as Bloch point singularities. The acquired extra topological phase (the Berry phase [28]) transforms the dynamics of magnons around these singular points and formally is equivalent to a quantum electrical charge dynamics in a magnetic field (for more details, see, e.g., Refs. [29,30]). Similarly, spin waves propagating through a skyrmion lattice can acquire a Berry phase due to the nonuniform static magnetization texture [31]. An example of a global-topological effect on magnetization dynamics is the shift of a magnon energy by an external electric field through the induced AC phase, the geometric phase acquired by chargeless quasiparticles with a magnetic dipole moment moving in an electric field. Note that an external electric field breaks the spatial inversion symmetry even if the original crystal symmetry of a magnet contains [25,32,33].

Zhang *et al.* [25] proved by the experimental data on centrosymmetric ferrite $Y_3Fe_5O_{12}$ (YIG) that the electric tuning of the SW phase in thin ferromagnet films can be realized with high efficiency. At an applied electric field of $\sim 10^6$ V/m, the phase shift (normalized to the propagation distance) was about 10^{-5} rad/mm [25]. This value can be drastically enhanced by decreasing wavelength. The experimental research of Serha *et al.* [32] also demonstrated that magnons could accumulate a geometrical phase by interacting with an electric field due to the AC effect, even in materials with a center of inversion symmetry. The authors used two types of magnetostatic SW propagating through an electric field region perpendicular and parallel to the film magnetization direction in YIG, revealing the AC effect's contribution to the SW phase change [32]. In thin YIG films, it is possible to reduce the crystal symmetry by the film shape, impurities, or a mismatch with the crystal lattice of the substrate. Based on the analysis of the experimental data, the authors [25,32] note that the SW's dynamic is mainly controlled by the magnonic AC effect and a magnetoelectric effect makes an insignificant contribution. The agreement of these experimental data with theoretical estimations points out that SWs can accumulate an additional phase through the magnonic AC effect and an external electric field can effectively control the SW power flux and caustics in thin ferromagnet films.

In this paper, we theoretically study the way to the efficient control and manipulation in real time of spin waves' dynamic properties in *insulating* AFM by an external electric field. We consider the AFM stripe to be in the x-z plane and an in-plane magnetic field $\mathbf{H}_0$ is parallel to the z axis (see Fig. 1); the static electric field and the wave vector of SWs are orthogonal to each other, $\mathbf{E} \perp \mathbf{k}$. In this geometry, the $\mathbf{E}$-field induced SWs phase shift is maximized, whereas the so-called Doppler shift due to an electric field vanishes (for more details, see

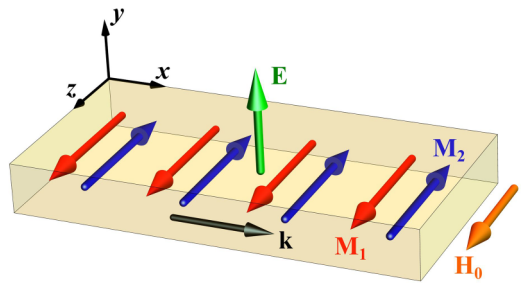

FIG. 1. Schematic representation of geometry and magnetic order of the AFM nanostripe under consideration. Red and blue arrows indicate magnetization of first and second sublattices along the z axis. The external electric field is normal to the film, $\mathbf{E} \parallel y$; spin waves propagate along the x axis, $\mathbf{k} \parallel x$, $\mathbf{H}_0 \parallel z$.

Refs. [16,34]). We focus on the case when the temperature is low and constant along the AFM stripe. Thus we analyzed the topological AC effect on the SWs dynamics in two-sublattice easy-axis antiferromagnetic insulators (AFMIs).

The following section starts with the model formulation and the phenomenological approach based on the well-known Landau-Lifshitz-Gilbert (LLG) equations for a two-sublattice easy-axis AFMI. The main results concerning the **E**-field topological effects of SW's dynamic in an AFMI are presented in Sec. III. The phenomenological description shows that, in a collinear AFMI, an external homogeneous **E** field leads to an asymmetric magnitude of the phase, the damping shifts for RH and LH SWs, and opens the possibility of a given chirality magnon ultrafast propagation at nanoscale distances. The AC effect on the so-called superluminal-like magnon propagation at nanoscale distances is also considered. Section IV is devoted to its discussions. We end with Conclusion and Acknowledgments.

II. THEORETICAL MODEL

Aharonov and Casher [27] predicted that a chargeless particle with a magnetic dipole, $\mathbf{m} = g\mu_B \mathbf{e}_z$ (g is the g factor and μ_B is the Bohr magneton), propagating in an external electric field **E** will acquire, in addition to a standard dynamic phase, a topological phase φ_{AC}. In a vacuum, the magnitude of the extra phase shift is proportional to $\sim(\mathbf{E} \times \mathbf{e}_z)(g\mu_B/\hbar c^2)$ and is extremely small (here c is the speed of light and $\hbar$ is the reduced Planck constant) [35,36]. Since a magnon possesses a magnetic dipole, $\mathbf{m} = \pm g\mu_B \mathbf{e}_z$, the question arises about the applicability of these results to a magnon moving in a material space, e.g., to a magnon moving in ideal magnetic insulator with the spatial inversion symmetry lattice. Microscopic theoretical estimation based on the superexchange model predicted that the electric-field-induced AC phase in magnetic insulators, e.g., such as YIG, is reasonably large to be experimentally detected [25,33,37–39]. In a linear approximation to the electric field, the effect of the **E** field-induced extra phase on a magnetization dynamics can be considered by adding a DM-like interaction between the magnetic moments $\mathbf{M}_i$ and $\mathbf{M}_j$ of neighboring ions that can be written in the traditional form as $\mathbf{d}_{ij} \cdot (\mathbf{M}_i \times \mathbf{M}_j)$. The vector $\mathbf{d}_{ij} \sim J\xi_{SO} e(\mathbf{E} \times \mathbf{e}_{ij})$ is perpendicular to the electric field **E** direction and to the vector $\mathbf{e}_{ij}$ along the line connecting the ions with $\mathbf{M}_i$ and $\mathbf{M}_j$ magnetic moments; here J is the exchange coupling, ξ_{SO} is the strength of the spin-orbit coupling between these ions, and e is the absolute value of the electron charge. The physical reason why the **E** field effect in this case is much larger than in a vacuum is that in a magnetic insulator the polarization of electronic orbitals (the electrons virtually hopping between the magnetic ions) by the electric field generates the spin-orbit coupling between the magnetic moments and thus an effective DM-like interaction.

Based on these predictions, we examine the **E** field effect on SWs propagating in a nanostripe of the AFMI with the centrosymmetric lattice. The magnetization moments $\mathbf{M}_1 = \mathbf{M}_1(\mathbf{r}, t)$ and $\mathbf{M}_2 = \mathbf{M}_2(\mathbf{r}, t)$ corresponding to the first and the second symmetric sublattices are directed oppositely along the z axis. The electric field is normal to the stripe, $\mathbf{E}||y$, and magnon propagation direction, $\mathbf{k}||x$; see Fig. 1. The total energy of the system, F, is

$$F = \int (E_{ex} + E_a + E_{ED} + E_H) dV \tag{1}$$

and consists of four components: the exchange E_{ex}, the magnetocrystalline anisotropy E_a, the electric-field-induced DM-like coupling E_{ED}, and the magnetic field E_H energy densities. We consider a general form of the exchange interaction, written in the continuum description as [12]

$$E_{ex} = J(\mathbf{M}_1\mathbf{M}_2) + \tfrac{1}{2}A[(\partial_x \mathbf{M}_1)^2 + (\partial_x \mathbf{M}_2)^2] + A_{12}(\partial_x \mathbf{M}_1)(\partial_x \mathbf{M}_2). \tag{2}$$

Here $J > 0$ stands for the homogeneous exchange coupling between sublattices; $A > 0$ and $A_{12} > 0$ are the inhomogeneous exchange intrasublattice and intersublattice coupling, respectively; $\partial_x = \partial/\partial x$. The uniaxial magnetocrystalline anisotropy energy, with a constant $K > 0$, is expressed as

$$E_a = -\tfrac{1}{2}K[(\mathbf{M}_1 \cdot \mathbf{e}_a)^2 + (\mathbf{M}_2 \cdot \mathbf{e}_a)^2] \tag{3}$$

and stabilizes the antiferromagnetic ordering with $\mathbf{M}_1 = -\mathbf{M}_2$ along the easy axis $\mathbf{e}_a||z$ [4].

A homogeneous static electric field $\mathbf{E}||y$ generates the DM-like interaction between magnetic moments of neighboring ions. This energy component, E_{ED}, can be presented in the conventional form

$$E_{ED} = \tfrac{1}{2}\mathbf{d}_{12} \cdot (\mathbf{M}_1 \times \mathbf{M}_2), \tag{4}$$

where the vector $\mathbf{d}_{12}$ is perpendicular to both the electric field **E** and the unit vector $\hat{\mathbf{e}}_{12}$ that is directed along the line that connects the magnetic moments $\mathbf{M}_1$ and $\mathbf{M}_2$. Microscopic calculations [25,33,37–39] give the following form of the vector $\mathbf{d}_{12}$:

$$\mathbf{d}_{12} = d_{AC}(\mathbf{E} \times \hat{\mathbf{e}}_{12}). \tag{5}$$

The material parameter, d_{AC}, depends on the strength of the exchange interaction and the spin-orbit coupling between the magnetic ions. In typical AFMs with antiparallel-coupled nearest magnetic moments, the effective intersublattice exchange interaction is much larger than the intrasublattice exchange interaction [3,4]. The strength of spin-orbit coupling between intersublattice magnetic moments is also larger in magnitude compared to the coupling between magnetic moments of the same sublattice due to the shorter interatomic

distance. Thus, following the results [25,33,37–39], we will suggest that the leading effective DM-like interaction in AFMI is $d_{AC} \sim \xi_{SO} Je$, where J is the intersublattice exchange coupling and ξ_{SO} is the strength of the spin-orbit coupling between the intersublattice magnetic moments. Compared with the exchange coupling, the d_{AC} magnitude is relatively weak and the applied electric field up to $|\mathbf{E}| \sim 100$ MV/m does not violate the uniform Néel ground state [25,33,37–39].

The last term in Eq. (1) accounts for the Zeeman energy of the external static magnetic field $\mathbf{H}_0$, which is parallel to the z axis:

$$E_H = -\mu_0 \mathbf{H}_0 (\mathbf{M}_1 + \mathbf{M}_2), \tag{6}$$

where μ_0 is the magnetic permeability of the vacuum.

The magnetization dynamics in AFMI is governed by the LLG equation of the form $\partial \mathbf{M}/\partial t = \gamma \mathbf{M} \times \mu_0 \partial F/\partial \mathbf{M} + \mathbf{R}$, where F is the total energy of the system, γ is the gyromagnetic ratio, and $\mathbf{R}$ is the relaxation term. In the standard LLG model, the relaxation term is written as $\alpha_G \mathbf{M}_i/M_0 \times \partial \mathbf{M}_i/\partial t$. Recent theoretical research on dissipative torques in two-sublattice magnets [40,41] suggested the important role of cross-sublattice Gilbert terms in the phenomenological description of SWs' damping. It was shown that the intersublattice damping can significantly influence the magnon's lifetime. We will consider the case when the Gilbert damping is captured by a viscous Rayleigh dissipation function parametrized by the damping constants α_{ij} $(i, j = 1, 2)$ that represent the dissipation rate of the magnetization $\mathbf{m_i} \times \frac{\partial \mathbf{m_j}}{\partial t}$ within intrasublattices, $i = j$, and cross-sublattices, $i \neq j$, assuming that the α_{ij} are spatially homogeneous and isotropic [40,41]. Hence the magnetization dynamics of a two-sublattice AFMI can be described by two coupled LLG equations with the intra- and intersublattice damping coefficients:

$$\begin{aligned}
\frac{\partial \mathbf{m_1}}{\partial t} &= -\gamma \mathbf{m_1} \times \mu_0 \mathbf{h_1} + \alpha_{11} \mathbf{m_1} \times \frac{\partial \mathbf{m_1}}{\partial t} + \alpha_{12} \mathbf{m_1} \times \frac{\partial \mathbf{m_2}}{\partial t}, \\
\frac{\partial \mathbf{m_2}}{\partial t} &= -\gamma \mathbf{m_2} \times \mu_0 \mathbf{h_2} + \alpha_{21} \mathbf{m_2} \times \frac{\partial \mathbf{m_1}}{\partial t} + \alpha_{22} \mathbf{m_2} \times \frac{\partial \mathbf{m_2}}{\partial t}.
\end{aligned} \tag{7}$$

Here $\mathbf{m}_i = \mathbf{M}_i/M_0$ $(i = 1, 2)$, $M_0 = |\mathbf{M}_1| = |\mathbf{M}_2|$ is the sublattice saturation magnetization, and $\mathbf{h_i} = -\partial F/\partial \mathbf{m_i}$ is the effective magnetic field acting on the sublattice. Below, we will suggest the AFMI is symmetric under sublattice permutation and the dissipation matrix is symmetric: $\alpha_{11} = \alpha_{22} = \alpha$, $\alpha_{12} = \alpha_{21} = \alpha_C$. The positivity of magnetization dynamics dissipation implies that $\alpha \geqslant \alpha_C > 0$ (see Refs. [40,41] for details).

We will focus on the electric-field-induced topological AC effect and will assume that (i) the AFM is a dielectric with the cubic symmetry lattice and (ii) the SW wave vector, $\mathbf{k}||x$, and the electric field, $\mathbf{E}||y$, are mutually orthogonal (see Fig. 1). In this geometry, the SW's Doppler shift vanishes (see, e.g., Ref. [34]) and it provides the maximum topological effect of an electric field on SW's dynamic.

There are two possible representations of the wave vector $\mathbf{k}$ and frequency ω for describing the magnetization dynamics in an absorbing medium: the complex frequency and real wave vector characterize the temporal decay of SW and the real frequency and complex wave vector characterize the spatial decay of a traveling SW; see Refs. [42–44]. The magnons propagation distance is significant in terms of their practical application. Considering the damping effect on SWs propagation length, we will use the real frequency and complex wave vector. Thus a small amplitude sublattices magnetization dynamic $\mathbf{m}_i$ around the static equilibrium is presented as

$$\mathbf{m}_i = m_{i0} \mathbf{e}_z + \mathbf{m}_{i(x,y)} \exp[-i(\omega t - kx)] \exp[-x/\Lambda], \tag{8}$$

where $\mathbf{m}_{i(x,y)} = (m_{ix}, m_{iy})$, $m_{i0} = \pm 1$, $|\mathbf{m}_{i(x,y)}| \ll 1$, k is the magnitude of the wave vector, and Λ is the SW's amplitude attenuation length.

In the spin-wave approximation, the equations of motion, Eq. (7), can be linearized. Substituting $\mathbf{m}_i$, Eq. (8), in Eq. (7), transferring to the conventional chiral variables $m_{1(2)\pm} = m_{1(2)x} \pm i m_{1(2)y}$, in the limit of long wavelength approximation, $ka \ll 1$ (a is the lattice constant), we obtain

$$\begin{pmatrix} \pm\omega\frac{M_0}{\gamma} + P + H_0 - i\alpha\omega\frac{M_0}{\gamma} & R_{\mp} - i\alpha_C\omega\frac{M_0}{\gamma} \\ R_{\mp} - i\alpha_C\omega\frac{M_0}{\gamma} & \mp\omega\frac{M_0}{\gamma} + P - H_0 - i\alpha\omega\frac{M_0}{\gamma} \end{pmatrix} \times \begin{pmatrix} m_{1\pm} \\ m_{2\pm} \end{pmatrix} = \begin{pmatrix} 0 \\ 0 \end{pmatrix}. \tag{9}$$

Here we used the notations $P = J + K + Ak^2$, $R_{\mp} = J + A_{12}k^2 \mp d_{AC}Ek$, and $k = k + i/\Lambda_{L/R}$. The magnons' dispersion relation and damping can be found as the eigenvalues of these matrix equations. In the following sections we discuss the **E**-field control of the right-handed spin-up and the left-handed spin-down SWs' asymmetric energy splitting, their propagation lengths, and the damping-induced group velocity anomaly.

III. CHIRALITY-SELECTIVE DYNAMICS: ELECTRIC-FIELD-INDUCED ASYMMETRIES IN FREQUENCY AND DECAY LENGTH OF SPIN WAVES

Frequency. In the spin-wave approximation, the magnons dispersion relation and damping can be found as the eigenvalues of the matrix equations, Eq. (9). Suggesting that the dissipation is zero, $\alpha = \alpha_C = 0$, and thus $\mathrm{Im}k = 0$, for the energy of the right-handed, ω_R, and the left-handed, ω_L, SWs propagating through an electric $\mathbf{E}||y$ and magnetic $\mathbf{H}_0||z$ fields region, we obtain

$$\omega_R(k, E) = \frac{\gamma}{M_0}\sqrt{[\varepsilon_m(k) + d_{AC}Ek][\varepsilon_l(k) - d_{AC}Ek]} + \gamma\mu_0 H_0, \tag{10}$$

$$\omega_L(k, E) = \frac{\gamma}{M_0}\sqrt{[\varepsilon_m(k) - d_{AC}Ek][\varepsilon_l(k) + d_{AC}Ek]} - \gamma\mu_0 H_0. \tag{11}$$

Here we introduce $\varepsilon_m(k) = [2J + K + (A + A_{12})k^2]$ and $\varepsilon_l(k) = [K + (A - A_{12})k^2]$. When $E = 0$, the magnetic field lifts the left- and right-handed SWs energy degeneracy splitting them on $2\gamma\mu_0 H_0$. The dependence of the magnon energy on the magnetic field is standard [4] and we temporarily (where not specified) set it to zero, $H_0 = 0$, but $E \neq 0$, to discuss the effects of the electric field. If the electric field is applied, the DM-like interaction is generated and the frequencies of the clockwise and counterclockwise SWs have been

separated. A stronger applied electric field results in a larger frequency difference for the two polarities. Note that changing the sign of the applied **E** field leads to a swap of the sign of the energy division between the left- and right-handed SWs. The energy splitting of the long-wave SWs is linearly dependent on the wave vector k and the applied electric field magnitude:

$$\omega_L(k,E)-\omega_R(k,E)=\frac{2\gamma J}{M_0\sqrt{\varepsilon_m(0)\varepsilon_l(0)}}d_{AC}Ek. \tag{12}$$

Figure 2(a) illustrates the evolution of the left- and right-handed long-wave magnons' energy dispersion under the electric field effect. The energy splitting dependence $\Delta\omega(k,E)=\omega_L(k,E)-\omega_R(k,E)$ between the right- and left-handed magnons on the wave vector k at different magnitudes of an electric field is shown in Fig. 2(b). The dependence of the SWs energy splitting $\Delta\omega(k,E)$ on the magnitude of the electric field at fixed wave vector k and magnetic field are shown in Fig. 2(c). Thus measurements of the SWs energy shift at $E\neq 0$ make it possible to determine the topological AC-phase magnitude.

The AFM parameters such as $KMnF_3$ have been used in graphical representations in Fig. 2 and others (see, e.g., Refs. [17,45]). Specifically, $M_0=3.76\times10^5$ A/m, $J=6.59\times10^{-12}$ a^2J/m^3, $A=0.5\times10^{-11}$ J/m, $A_{12}=0.4\times10^{-11}$ J/m, $K=1.16\times10^5$ J/m^3, $a=0.418$ nm, and $\gamma=1.76\times10^{11}$ rad Hz/T. The DM-like constant d_{AC} is a parameter in our model and we take $d_{AC}=4.4\times10^{-12}$ C/m [25,26,39]; the damping coefficients are $\alpha=0.002$ and $\alpha_C=0.001$.

The E-field control of SW propagation length. The external electric field also affects the propagation distance of left- and right-handed magnons. Setting the imaginary part of the determinant Eq. (9) to zero and taking into account the dissipation, $k=k+i/\Lambda_{L/R}$, we find the long-wavelength SWs damping length in the following form (Λ_L upper sign and Λ_R lower sign):

$$\Lambda_{L/R}(k,E)=\frac{\gamma}{M_0\omega_{L/R}(k,E)}\frac{c_1k\pm d_{AC}E(J+3A_{12}k^2)}{\alpha(J+K)-\alpha_C(J\mp d_{AC}Ek)}, \tag{13}$$

where $c_1=2AK-(d_{AC}E)^2+2J(A-A_{12})$. Thus the SWs' attenuation lengths are asymmetric $\Lambda_{R/L}(k)\neq\Lambda_{R/L}(-k)$ and demonstrate the chirality dependence. The electric field increases or decreases the propagation lengths of given chirality magnons if their propagation is changed in the opposite direction. The largest difference in the propagation length (and the lifetime) is between the long-wavelength magnons ($k\to0$):

$$[\Lambda_L(k,E)-\Lambda_R(k,E)]|_{k\to0}|=\frac{2}{\sqrt{\varepsilon_m(0)\varepsilon_l(0)}}\frac{Jd_{AC}E}{\alpha(J+K)-\alpha_CJ}. \tag{14}$$

The dependency of the attenuation length on the frequency of the LH and RH SWs at $E=50$ V/μm is shown in Fig. 3(a). The attenuation length of one chirality of the SW mode increases faster than the other. If the sign of the **E** field changes, the left- and right-handed SW decay length swap places. The magnetic field $\mu_0H_0=0.2$ T amplifies the electric field effect on the attenuation and leads to $\Delta\Lambda(k,E)=\Lambda_L(k,E)-\Lambda_R(k,E)$ increasing. If the sign of the magnetic field is reversed, the sign of $\Delta\Lambda(k,E)$ is reversed too when

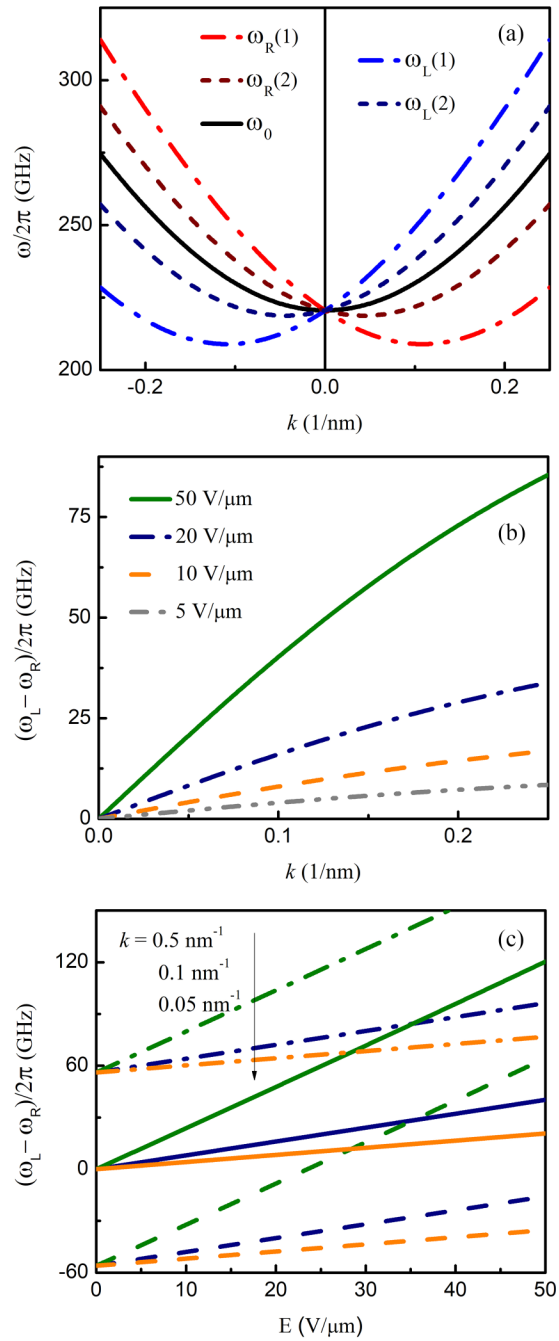

FIG. 2. (a) Right-handed ω_R (red line) and left-handed ω_L (blue line) spin waves energy dispersion under the **E**-field effect: (1) $E=50$ V/μm (dash-dotted lines); (2) $E=20$ V/μm (dashed lines). The black solid line ω_0 corresponds to $E=0$. $H_0=0$. (b) The energy splitting $\Delta\omega(k,E)=\omega_L(k,E)-\omega_R(k,E)$ between the right-handed and the left-handed long-wave magnons on the wave vector **k** at the electric field: $E=50$ V/μm ($\Delta\omega_1$), 20 V/μm ($\Delta\omega_2$), 10 V/μm ($\Delta\omega_3$), and 5 V/μm ($\Delta\omega_4$). $H_0=0$. (c) The dependence of the energy splitting $\Delta\omega(k,E)=\omega_L(k,E)-\omega_R(k,E)$ on the magnitude of the electric field at different wave vectors: $k=0.5$ nm^{-1} (green lines), $k=0.1$ nm^{-1} (blue lines), and $k=0.05$ nm^{-1} (orange lines). $H_0=0$ (solid lines), $\mu_0H_0=-1$ T (dotted lines), and $\mu_0H_0=1$ T (dashed lines).

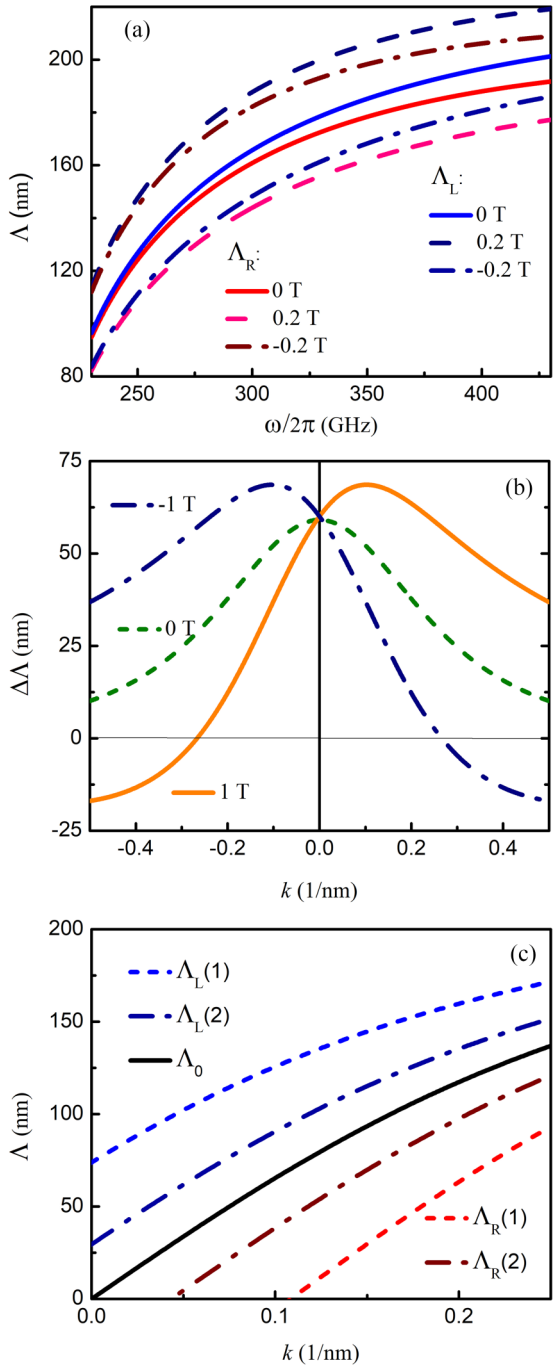

FIG. 3. (a) Attenuation length frequency dependence of the right-handed $\Lambda_R(\omega, E)$ (red lines) and the left-handed $\Lambda_L(\omega, E)$ (blue lines) spin waves at the electric field $E = 50$ V/μm. The magnetic field: $H_0 = 0$ (solid lines), $\mu_0 H_0 = 0.2$ T (dashed lines), and $\mu_0 H_0 = -0.2$ T (dot-dashed lines). (b) The spin waves attenuation length difference, $\Delta\Lambda(k, E) = \Lambda_L(k, E) - \Lambda_R(k, E)$, depends on the wave vector at different magnetic fields: $H_0 = 0$ (dashed line), $\mu_0 H_0 = 1$ T (solid line), and $\mu_0 H_0 = -1$ T (dotted line). $E = 20$ V/μm. (c) The damping length with an applied electric field: (1) $E = 50$ V/μm; (2) $E = 20$ V/μm. Black line corresponds to $E = 0$. $\alpha = 0.002$; $\alpha_C = 0.001$.

$\mathbf{E} = 0$. Figure 3(b) illustrates the dependence of the attenuation length difference, $\Lambda_L(k, E) - \Lambda_R(k, E)$, on a small k at $\mathbf{E} \neq 0$ without and at applied magnetic field. When $\mathbf{H}_0 = 0$, we have $\Delta\Lambda(k, E) = \Delta\Lambda(-k, E)$. After reaching the maximum value at $k \to 0$, $\Delta\Lambda(k, E)$ decreases gradually up to the Brillouin zone boundary. The application of the magnetic field causes the difference in the attenuation lengths of SWs propagating in the opposite direction. The magnetic field also affects the LH and RH SWs damping in the absence of an electric field.

Note also, as the theory points out [40,41], the SWs damping reduces with increasing the intersublattices damping α_C (but keeping the ratio $\alpha_C \leqslant \alpha$). This antidamping effect of the intersublattices damping also persists when an electric field is applied: the cross-sublattices damping α_C increases the SW's damping length (the lifetime) of both chiralities; see Eqs. (13) and (14).

The E-field effect on SW's group velocity. The SW group's velocity in magnetic nanoheterostripes is a significant factor in the magnonic device speed operation. In the absence of damping, the RH and LH magnons' group velocity $\upsilon_{R/L}(k, E) = d\omega_{R/L}(k, E)/dk$ is

$$\upsilon_{L/R}(k, E) = \left(\frac{\gamma}{M_0}\right)^2 \frac{c_1 k \pm d_{AC} E J \pm 3 d_{AC} E A_{12} k^2 + 2k^3 \left(A^2 - A_{12}^2\right)}{\omega_{L/R}(k, E)}. \tag{15}$$

In the long-waves limit, neglecting small terms proportional k^2 and d_{AC}^2, one finds

$$[\upsilon_L(k, E) - \upsilon_R(k, E)]|_{k \to 0} = \frac{2 J d_{AC} E}{M_0 \sqrt{\varepsilon_m(0)\varepsilon_l(0)}}. \tag{16}$$

Thus the external $\mathbf{E}$ field generates artificial DM interaction and asymmetrically splits the group velocity of LH and RH SWs. By changing the $\mathbf{E}$-field sign, the sign of the asymmetry SWs' group velocity is changed too.

The significant interest in SW's group velocity is motivated by the prospects of ultrafast nanodevices exploiting AFMs for spintronics. Since the group velocity characterizes the speed at which data transfers from one computer component to another, understanding its limits is an exciting area of research. As theory predicted [42,43] in the presence of damping, the magnon dispersion can be anomalous and the long-wavelength SW's group velocity can be much larger than in the absence of damping. Recent studies have estimated that the SWs' velocity in AFMs can be around 10–100 km/s [9,46,47]. In this context, observing a magnon velocity of up to 650 km/s in AFM insulator NiO [44] is pioneering and impressive. The authors called the observed effect a superluminal-like magnon propagation. Thus the question arises: how does the topological AC phase affect the superluminal-like magnon propagation?

IV. SUPERLUMINAL-LIKE MAGNON PROPAGATION

Following the experimental results in Ref. [44], and to explore the potential anomalous behavior of frequency and velocity more deeply, we will consider more accurate terms proportional to $1/\Lambda$ in the determinant of Eq. (9). First, we revise the relationship between the two parameters of the SW's propagation: the SW's vector k real part and its damping

length Λ or the inverse of the imaginary part of the SW vector $\Lambda = 1/k_{im}$. Setting the imaginary part of the determinant Eq. (9) to zero and taking into account the dissipation like for Eq. (13) with respect to Λ we get (Λ_L upper sign and Λ_R lower sign)

$$\Lambda_{L/R}(k,E) = c_1 \frac{\gamma}{M_0 \tilde{\omega}_{L/R}(k,E)} \frac{k \pm k_0}{[\alpha(J+K) - \alpha_C J]}. \quad (17)$$

The constant $k_0 = J d_{AC} E/c_1$ describes the chirality-dependent shift of the minimum SW's energy along the wave vector's axis—the **E**-field topological effect. Equation (17) refines (corrects) Eq. (13) in the vicinity k_0: a finite damping causes a sharp dip in the frequency $\tilde{\omega}_{L/R}(k,E)$ around k_0 (see below). The graphics for $\Lambda_{L/R}(k,E)$ for Eqs. (13) and (17) are almost the same and presented on Fig. 3(c). Nevertheless, this will play a role for frequency and group velocity. Below we will show how accounting the imaginary part of the wave vector, namely $\sim 1/\Lambda^2$, into the real frequency influences the SW dynamics and leads to the appearance of a region with anomalous behavior.

To consider the damping effect on the magnon dispersion in the long wavelength limit, we will suggest that $1/\Lambda \sim k$, but still $a/\Lambda \sim ak \ll 1$. It means that the equation for the real part of determinant, Eq. (9), has new terms $\sim 1/\Lambda^2$. Inserting this expression for $\Lambda(k,E)$, Eq. (17), into the real part of the determinant Eq. (9) we will get the frequency

$$\tilde{\omega}_{L/R}(k,E) = \frac{\gamma(k \pm k_0)}{M_0} \sqrt{\frac{c_1[c_2 + (k \pm k_0)^2]}{\alpha_i\left[(k \pm k_0)^2 + 2c_4(k \pm k_0) + c_3\right]}}, \quad (18)$$

where $c_2 = K(K+2J)/c_1 - k_0^2$, $c_3 = [\alpha(K+J) - \alpha_C J]^2/\alpha_i c_1$, $c_4 = \alpha_C d_{AC} E[\alpha(K+J) - \alpha_C J]/\alpha_i c_1$, and $\alpha_i = 1 + \alpha^2 - \alpha_C^2$. Considering the damping parameters magnitude $\sim 10^{-3}$–10^{-4}, further, we will suggest $\alpha_i \simeq 1$. Figure 4 shows the difference between the frequencies derived from Eqs. (10), (11), and (18). A finite damping causes a sharp dip around $k = k_0$ and $k = -k_0$ in $\tilde{\omega}_R(k,E)$ and $\tilde{\omega}_L(k,E)$, respectively. This anomalous magnon dispersion behavior appears due to taking into account the terms proportional to $1/\Lambda^2$.

The anomalous decrease in $\tilde{\omega}_{L/R}(k,E)$ results in an anomalous increase of the magnon group velocity. At small wave numbers $\tilde{\upsilon}_{L/R}(k,E)$ is

$$\tilde{\upsilon}_{L/R}(k,E) = \frac{\gamma\sqrt{c_1}}{M_0} \frac{(k \pm k_0)^4 + 3c_4(k \pm k_0)^3 + 2c_3(k \pm k_0)^2 + c_2 c_4(k \pm k_0) + c_2 c_3}{\sqrt{\alpha_i}[(k \pm k_0)^2 + 2c_4(k \pm k_0) + c_3]^{3/2}\sqrt{c_2 + (k \pm k_0)^2}} \quad (19)$$

and is larger than $\upsilon_{L/R}(k,E)$, Eq. (15). For the AFMI magnetic parameters we used, at nanoscale distance the values of the group velocity $\tilde{\upsilon}_{L/R}(k,E)$ could be around 320 km/s; that is extremely high compared to the values from the previous section, Eq. (15), where group velocity is two orders times lower in this region. That is so-called superluminal-like magnon propagation [44]. Considering the fact that authors [44] have shown the experiment with high velocity and made some theoretical predictions using a similar idea, this opens the perspective for higher group velocities than previously expected. Moreover, it points out that we should pay more attention to the dissipation effects in SW's dynamics even when SW's damping in insulating AFM is very small. Figure 5 shows the difference between group velocities calculated from Eqs. (15) and (19). There is almost no difference between expressions for the frequency, damping length, and group velocity for most values of the wave vector

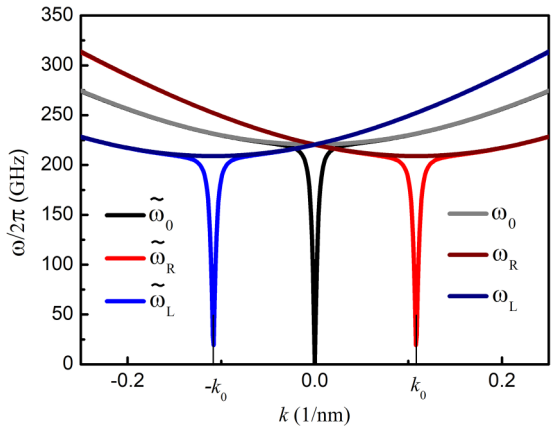

FIG. 4. Damping-induced dispersion of the right-handed $\tilde{\omega}_R(k,E)$ (red line) and the left-handed $\tilde{\omega}_L(k,E)$ (blue line) spin waves at the electric field $E = 50$ V/μm and $E = 0$ (black line). There is no anomalous behavior of SW's dispersion when $\alpha = \alpha_C = 0$: ω_R, ω_L, and ω_0 [Eqs. (10) and (11)].

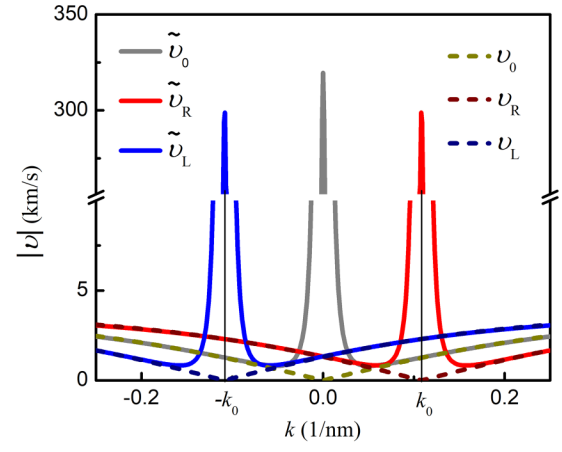

FIG. 5. Magnitude of damping-induced superluminal-like magnon group velocity. Solid lines, Eq. (19): the right-handed $\tilde{\upsilon}_R(k,E)$ (red line) and the left-handed $\tilde{\upsilon}_L(k,E)$ (blue line) at the electric field $E = 50$ V/μm and $\tilde{\upsilon}_0(k)$ at $E = 0$ (black line). Dashed lines, Eq. (15): $\upsilon_R(k,E)$, $\upsilon_L(k,E)$, and υ_0 at the electric field $E = 50$ V/μm and at $E = 0$, respectively.

k except a small region around k_0. The width of a sharp dip depends on the main quantities of the material, but its position, $k_0 = \pm J d_{AC} E/c_1$, can be controlled by the external **E** field. Figures 4 and 5 show how the external **E** field can dramatically change the kinetic properties of magnons, such as the wave vector at which the superluminal propagation of a given chirality magnon occurs. This chirality-selective topological effect on superluminal propagation SWs behavior paves the way for the development of advanced magnonic devices.

V. CONCLUSION

Two types of SWs chirality, the right- and left-handed modes, exist in the antiferromagnetic structures due to two antiparallel magnetization sublattices. In systems with broken inversion symmetry and strong spin-orbit coupling, the antisymmetric component of exchange interaction, known as the DM interaction, generates an asymmetric SW dispersion $\omega_{L/R}(k) \neq \omega_{L/R}(-k)$: magnons propagating in opposite directions have different phase, amplitude, and attenuation. These stimulated researchers to use SWs of different chirality and their nonreciprocity in magnonic devices. The effect of nonreciprocity could be applied to such magnonic devices as SW field-effect transistors, diodes, directional SW emitters, passive nonreciprocal filters, etc. [5,34,47,48]. Applying a magnetic field can solve the SW spectrum handedness splitting. Nevertheless, an electric field could be a more efficient way of controlling the SWs' chirality-selective dynamics. Liu *et al.* [49] have demonstrated the electric-field-induced switching of magnon spin current polarization by varying a gate voltage in the antiferromagnetic insulator Cr_2O_3. Electric field control of SWs in different thicknesses of CoFeB films has also been observed in Ref. [50].

According to the paradigm of quantum physics, controlling magnetization dynamics through modification of the system's magnetic parameters implies a modification of the local (Landau) order parameters. In recent years, condensed matter physics has been revolutionized by introducing topology-grounded concepts that characterize physical states and properties by global nonlocal quantities, which endow the system with global stability to perturbations. In magnetism, the topological concepts can be conditionally divided into two different scenarios: (i) a nontrivial topology of a static magnetic order in the real space, e.g., magnetic structures such as skyrmions, magnetism in curved geometries, etc., and (ii) topological effects in magnetization dynamics. The electric field's topological effect on magnon dynamics provides a promising platform for developing ultrafast topological magnonics. The theoretically predicted phenomenon [51–54] of the change of the SW's phase due to the magnonic Aharonov-Casher effect—the accumulation of the topological phase by a quantum orbital motion of chargeless bosonic quasiparticles with magnetic dipole moment in an electric field region—was already obtained with convincing evidence in experiments on YIG [25,32]. In a collinear AFMI, the external **E** field leads to an asymmetric magnitude of the phase shift and damping for the right-handed and the left-handed chirality magnons. This provides a way to manipulate the spin-up and spin-down SWs' dynamical phase and their attenuation length in AFMIs via an external electric field, developing another direction in the field of antiferromagnetic magnonics—non-Abelian magnonics in AFM insulators [55].

We have theoretically studied the effect of the quantum Aharonov-Casher phase on the possibility of directly controlling the phase and the attenuation of the right-handed and the left-handed spin waves in a dielectric collinear antiferromagnet by an external electric field. The magnonic AC phase is purely a quantum effect and can be accounted for by adding the Dzyaloshinskii-Moriya-like interaction between neighboring spins. Analytical calculations demonstrate that the electric field can successfully manage the right-handed and left-handed spin wave spectrum, amplitude, and propagation length without adding the magnetic field. The attenuation of the given chirality magnons can be enhanced or weakened separately depending on the direction and magnitude of the electric field. A finite damping makes the magnon's dispersion anomalous, e.g., a giant magnon velocity at nanoscale distances. An external electric field can control the position of this superluminal-like magnon velocity region. Effective control of a given chirality spin wave's phase, amplitude, and speed provides a way to design a magnonic device. We hope the obtained results will contribute to the fundamental understanding of topological effects in the chirality-dependent spin wave dynamics in collinear antiferromagnetic insulators in different energy ranges that can be a key factor for designing quantum magnonic devices.

ACKNOWLEDGMENTS

The authors acknowledge A. Savchenko for useful discussions and for helpful and valuable comments on the manuscript. The work was supported by the STCU, project "Magnetism in Ukraine Initiative," Project Agreement No. 9918. O.O.B. gratefully acknowledges support from BMBF through the GU-QuMat project (No. 01DK24008).

[1] V. V. Kruglyak, S. O. Demokritov, and D. Grundler, Magnonics, J. Phys. D: Appl. Phys. **43**, 264001 (2010).

[2] A. V. Chumak, V. I. Vasyuchka, A. A. Serga, and B. Hillebrands, Magnon spintronics, Nat. Phys. **11**, 453 (2015).

[3] F. Kefer and C. Kittel, Theory of antiferromagnetic resonance, Phys. Rev. **85**, 329 (1952).

[4] A. I. Akhiezer, V. G. Bar'yakhtar, and S. V. Peletminskii, *Spin Waves* (North-Holland Publishing Company, Amsterdam, 1968).

[5] R. Cheng, M. W. Daniels, J.-G. Zhu, and D. Xiao, Antiferromagnetic spin wave field-effect transistor, Sci. Rep. **6**, 24223 (2016).

[6] E. V. Gomonay and V. M. Loktev, Spintronics of antiferromagnetic systems (review article), Low Temp. Phys. **40**, 17 (2014).

[7] C. Jia, M. Chen, A. F. Schäffer, and J. Berakdar, Chiral logic computing with twisted antiferromagnetic magnon modes, npj Comput. Mater. **7**, 101 (2021).

[8] V. Baltz, A. Manchon, M. Tsoi, T. Moriyama, T. Ono, and Y. Tserkovnyak, Antiferromagnetic spintronics, Rev. Mod. Phys. **90**, 015005 (2018).

[9] J. R. Hortensius, D. Afanasiev, M. Matthiesen, R. Leenders, R. Citro, A. V. Kimel, R. V. Mikhaylovskiy, B. A. Ivanov, and A. D. Caviglia, Coherent spin-wave transport in an antiferromagnet, Nat. Phys. **17**, 1001 (2021).

[10] J. Han, R. Cheng, L. Liu, H. Ohno, and S. Fukami, Coherent antiferromagnetic spintronics, Nat. Mater. **22**, 684 (2023).

[11] T. Satoh, S.-J. Cho, R. Iida, T. Shimura, K. Kuroda, H. Ueda, Y. Ueda, B. A. Ivanov, F. Nori, and M. Fiebig, Spin oscillations in antiferromagnetic NiO triggered by circularly polarized light, Phys. Rev. Lett. **105**, 077402 (2010).

[12] I. Proskurin, R. L. Stamps, A. S. Ovchinnikov, and J. I. Kishine, Spin-wave chirality and its manifestations in antiferromagnets, Phys. Rev. Lett. **119**, 177202 (2017).

[13] S.-J. Lee, D.-K. Lee, and K.-J. Lee, Effect of inhomogeneous Dzyaloshinskii-Moriya interaction on antiferromagnetic spin-wave propagation, Phys. Rev. B **101**, 064422 (2020).

[14] T. H. Kim, P. Grüenberg, S. H. Hang, and B. K. Cho, Field-driven dynamics and time-resolved measurement of Dzyaloshinskii-Moriya torque in canted antiferromagnet $YFeO_3$, Sci. Rep. **7**, 4515 (2017).

[15] Zh. Yan, Zh. Li, X. Wang, Z. Luo, Q. Xia, Y. Nie, and G. Guo, Manipulation of spin-wave attenuation and polarization in antiferromagnets, Phys. Rev. B **108**, 134432 (2023).

[16] V. Vlaminck and M. Bailleul, Current-induced spin-wave doppler shift, Science **322**, 410 (2008).

[17] V. Puliafito, R. Khymyn, M. Carpentieri, B. Azzerboni, V. Tiberkevich, A. Slavin, and G. Finocchio, Micromagnetic modeling of terahertz oscillations in an antiferromagnetic material driven by the spin Hall effect, Phys. Rev. B **99**, 024405 (2019).

[18] D.-H. Kim, S.-H. Oh, D.-K. Lee, S. K. Kim, and K.-J. Lee, Current-induced spin-wave Doppler shift and attenuation in compensated ferrimagnets, Phys. Rev. B **103**, 014433 (2021).

[19] R. Cheng, S. Okamoto, and D. Xiao, Spin nernst effect of magnons in collinear antiferromagnets, Phys. Rev. Lett. **117**, 217202 (2016).

[20] V. A. Zyuzin and A. A. Kovalev, Magnon spin nernst effect in antiferromagnets, Phys. Rev. Lett. **117**, 217203 (2016).

[21] K. Nakata, S. K. Kim, and Sh. Takayoshi, Laser control of magnonic topological phases in antiferromagnets, Phys. Rev. B **100**, 014421 (2019).

[22] Y. D. Wang, Z.-G. Zhu, and G. Su, Magnon spin photogalvanic effect induced by Aharonov-Casher phase, Phys. Rev. B **110**, 054434 (2024).

[23] Y. D. Wang, Zh.-G. Zhu, and G. Su, Magnon Landau-Zener tunneling and spin-current generation by electric field, Phys. Rev. B **111**, 165150 (2025).

[24] K. Nakata, S. K. Kim, J. Klinovaja, and D. Loss, Magnonic topological insulators in antiferromagnets, Phys. Rev. B **96**, 224414 (2017).

[25] X. Zhang, T. Liu, M. E. Flatté, and H. X. Tang, Electric-field coupling to spin waves in a centrosymmetric ferrite, Phys. Rev. Lett. **113**, 037202 (2014).

[26] V. Basso and P. Ansalone, Electric field effect on spin waves: Role of magnetic moment current, Europhys. Lett. **130**, 17008 (2020).

[27] Y. Aharonov and A. Casher, Topological quantum effects for neutral particles, Phys. Rev. Lett. **53**, 319 (1984).

[28] M. V. Berry, Quantum phase factors accompanying adiabatic changes, Proc. R. Soc. Lon. A **392**, 45 (1984).

[29] R. G. Elías, V. L. Carvalho-Santos, A. S. Núñez, and A. D. Verga, Spin waves scattering on a Bloch point, Phys. Rev. B **90**, 224414 (2014).

[30] A. Tapia, C. Saji, A. Roldán-Molina, and A. S. Nunez, Stability enhancement by zero-point spin fluctuations: a quantum perspective on bloch point topological singularities, Adv. Funct. Mater. **34**, 2312721 (2024).

[31] A. Roldán-Molina, A. S. Nunez, and J. Fernández-Rossier, Topological spin waves in the atomic-scale magnetic skyrmion crystal, New J. Phys. **18**, 045015 (2016).

[32] R. O. Serha, V. I. Vasyuchka, A. A. Serga, and B. Hillebrands, Towards an experimental proof of the magnonic Aharonov-Casher effect, Phys. Rev. B **108**, L220404 (2023).

[33] T. Liu and G. Vignale, Electric control of spin currents and spin-wave logic, Phys. Rev. Lett. **106**, 247203 (2011).

[34] J. Fernández-Rossier, M. Braun, A. S. Núñez, and A. H. MacDonald, Influence of a uniform current on collective magnetization dynamics in a ferromagnetic metal, Phys. Rev. B **69**, 174412 (2004).

[35] R. Mignani, Aharonov-Casher effect and geometrical phases, J. Phys. A: Math. Gen. **24**, L421 (1991).

[36] F. Meier and D. Loss, Magnetization transport and quantized spin conductance, Phys. Rev. Lett. **90**, 167204 (2003).

[37] Xi. Wang, L. Chotorlishvili, G. Guo, and J. Berakdar, Electric field controlled spin waveguide phase shifter in YIG, J. Appl. Phys. **124**, 073903 (2018).

[38] H. Katsura, N. Nagaosa, and A. V. Balatsky, Spin current and magnetoelectric effect in noncollinear magnets, Phys. Rev. Lett. **95**, 057205 (2005).

[39] T. Liu and G. Vignale, Flexoelectric phase shifter for spin waves, J. Appl. Phys. **111**, 083907 (2012).

[40] A. Kamra, R. E. Troncoso, W. Belzig, and A. Brataas, Gilbert damping phenomenology for two-sublattice magnets, Phys. Rev. B **98**, 184402 (2018).

[41] H. Y. Yuan, Q. Liu, K. Xia, Zh. Yuan, and X. R. Wang, Proper dissipative torques in antiferromagnetic dynamics, Europhys. Lett. **126**, 67006 (2019).

[42] Y. Tserkovnyak, Exceptional points in dissipatively coupled spin dynamics, Phys. Rev. Res. **2**, 013031 (2020).

[43] M. Dehmollaian and C. Caloz, General mapping between complex spatial and temporal frequencies by analytical continuation, IEEE Trans. Antennas Propag. **69**, 6531 (2021).

[44] K. Lee, D.-K. Lee, D. Yang, R. Mishra, D.-J. Kim, S. Liu, Q. Xiong, S. K. Kim, K.-J. Lee, and H. Yang, Superluminal-like magnon propagation in antiferromagnetic NiO at nanoscale distances, Nat. Nanotechnol. **16**, 1337 (2021).

[45] J. Barker and O. A. Tretiakov, Static and dynamical properties of antiferromagnetic skyrmions in the presence of applied current and temperature, Phys. Rev. Lett. **116**, 147203 (2016).

[46] R. V. Ovcharov, B. A. Ivanov, J. Åkerman, and R. S. Khymyn, Emission of fast-propagating spin waves by an antiferromagnetic domain wall driven by spin current, Phys. Rev. B **109**, L140406 (2024).

[47] O. Gomonay, T. Jungwirth, and J. Sinova, High antiferromagnetic domain wall velocity induced by Néel spin-orbit torques, Phys. Rev. Lett. **117**, 017202 (2016).

[48] R. K. Shukla, L. Chotorlishvili, V. Vijayan, H. Verma, A. Ernst, S. S. P. Parkin, and S. K. Mishra, Quantum information

diode based on a magnonic crystal, Mater. Quantum Technol. **3**, 035003 (2023).

[49] C. Liu, Y. Luo, D. Hong, S. S.-L. Zhang, H. Saglam, Yi Li, Y. Lin, B. Fisher, J. E. Pearson, J. S. Jiang, H. Zhou, J. Wen, A. Hoffmann, and A. Bhattacharya, Electric field control of magnon spin currents in an antiferromagnetic insulator, Sci. Adv. **7**, eabg1669 (2021).

[50] B. Rana, S. Choudhury, K. Miura, H. Takahashi, A. Barman, and Y. C. Otani, Electric field control of spin waves in ultrathin CoFeB films, Phys. Rev. B **100**, 224412 (2019).

[51] K. Nakata, P. Simon, and D. Loss, Spin currents and magnon dynamics in insulating magnets, J. Phys. D: Appl. Phys. **50**, 114004 (2017).

[52] V. N. Krivoruchko, A. S. Savchenko, and V. V. Kruglyak, Electric-field control of spin-wave power flow and caustics in thin magnetic films, Phys. Rev. B **98**, 024427 (2018).

[53] A. Savchenko and V. Krivoruchko, Electric-field control of nonreciprocity of spin wave excitation in ferromagnetic nanostripes, J. Magn. Magn. Mater. **474**, 9 (2019).

[54] V. N. Krivoruchko and A. S. Savchenko, Controlled refraction and focusing of spin waves determined by the Aharonov-Casher effect, Phys. Rev. B **109**, 184437 (2024).

[55] M. W. Daniels, R. Cheng, W. Yu, J. Xiao, and Di Xiao, Nonabelian magnonics in antiferromagnetis, Phys. Rev. B **98**, 134450 (2018).